The 2013 World Congress on
Advances in Structural Engineering and Mechanics (ASEM13)
Jeju, Korea, September 8-12, 2013

Ballistic behavior of steel sheets subjected to impact and perforation

*T. Jankowiak[1)], K.M. Kpenyigba[2)], R. Pesci[3)] , A. Rusinek[4)]

[1)]*Institute of Structural Engineering, PUT, Poznan, Poland*
[2), 4)]*LaBPS, National Engineering School of Metz, Metz, France*
[3)] *LEM3 UMR CNRS 7239, ENSAM-Arts et Métiers ParisTech CER of Metz, Metz, France*
[1)] tomasz.jankowiak@put.poznan.pl

ABSTRACT

The paper is reporting some comparisons between experimental and numerical results in terms of failure mode, failure time and ballistic properties of mild steel sheets. Several projectile shapes have been considered to take into account the stress triaxiality effect on the failure mode. The initial and residual velocities are also measured and the impact force is analyzed using numerical simulations.

1. INTRODUCTION

The paper describes the behavior of mild steel sheets under extreme loading conditions. Previously, the topic was developed by many authors as for example Zukas and Sheffler. The authors analyzed the perforation of the monolithic and multi-layered slabs using two descriptions of deformations: Lagrangian and Eulerian. It was illustrated that Lagrangian formulation predicts more accurate results than Eulerian when comparing experimental data with analytical solutions (Zukas 2001). Scheffler and Zukas analyzed influence of two numerical methods: finite difference (FD) and finite element (FE) on numerical results for fast dynamic problems. The authors illustrated the origin of the discrepancy in numerical results. The distribution of nodes (FD), shape and type of elements (FE) were taken into account. The authors also previously described the effect on the dynamic behavior of the metal sheets of the contact interaction formulation and of the constitutive material description (strain rate sensitivity type) (Scheffler 2000). Dean, Dunleavy, Brown and Clyne analyzed the ballistic properties of thin steel sheets using Abaqus/Explicit finite element code for

[1)] Associate Professor
[2)] PhD student
[3)] Associate Professor
[4)] Professor

projectile impact velocities between 200 and 600m/s. The energetic balance during the penetration and perforation of the structure by hemispherical projectiles was illustrated using the shell finite elements description for steel sheets (Dean 2009). Lee and Wierzbicki presented the propagation of radial cracks in thin metal sheets during impact by impulsive loads. The authors analyzed the influence of the triaxiality on the failure pattern using the shell elements for impacted structure (Lee 2005). Atkins, Afzal Khan and Liu analyzed the formation of radial cracks around the perforation zone in aluminum sheets. The influence of the small hole in the impacted area was taken into account for both conical and hemispherical projectiles. The authors observed that the appearance of the cracks is preluded by the creation of necks. In addition, they observed that the number of cracks is smaller than the number of necks (Atkins 1998). Other authors analyzed the perforation of thick plates. Borvik, Hopperstad, Berstad and Langseth presented the influence of the projectile end shape on the failure pattern during perforation of 12mm steel sheets (Weldox 460 E). They illustrated the influence of the projectile shape on the absorbed energy. A lower energy is absorbed during impact of the blunt projectile, Fig. 1 (Borvik 2002). Dey, Borvik, Hopperstad, Leinumand and Langseth analyzed the perforation of 12mm steel plates for different types of Weldox steel. The different shapes of projectiles were studied and their influence on the ballistic properties were illustrated. The identification of the material parameters based on different tests, static and dynamic (Jankowiak 2013), were presented (Dey 2004). The other authors analyzed the multilayered structures perforated by hemispherical projectiles. Alavi Nia and Hoseini described that monolitic structures are much more resistant to perforation (lower residual velocity and higher ballistic limit) than multilayered (Alavi Nia 2011). Jankowiak, Rusinek and Wood presented a numerical study of the perforation process of mild steel sheets for conical projectiles (Jankowiak 2013). The authors studied different configurations (also multilayered) of steel sheets and the two constitutive models: Rusinek-Klepaczko (Rusinek 2000, Rusinek 2007) and Johnson-Cook (Johnson 1983). The effects of the material behavior, strain rate sensitivity, yield stress and strain hardening were illustrated. Recht and Ipson presented an analytical equation for approximation of the ballistic curve. It is validated for perpendicular and oblique impacts using different projectile shapes (Recht 1963). This paper describes extensions of the previous works and presents an analysis based on the failure time and impact force for different kinds of projectiles. It contains two main parts: experimental and numerical results as following.

2. EXPERIMENTAL PART

The experimental technique is presented below in details. All tests are performed to describe the ballistic dynamic behavior of the steel sheets.

2.1 Description of experiments

The tested structure is a mild steel sheet. The dimensions of the plate are 130x130mm^2 with a thickness equal to 1mm. The steel sheet is fixed during perforation with an active part of 100x100mm^2, Fig. 1. Other dimensions are reported on the picture. The process can be divided into three main stages which are defined by the position of the projectile:

- impact into the structure,
- penetration of the structure (initially only projectile nose),
- perforation of the structure.

The process is carefully recorded using a High Speed Camera (HSC) Phantom v711 during experiments.

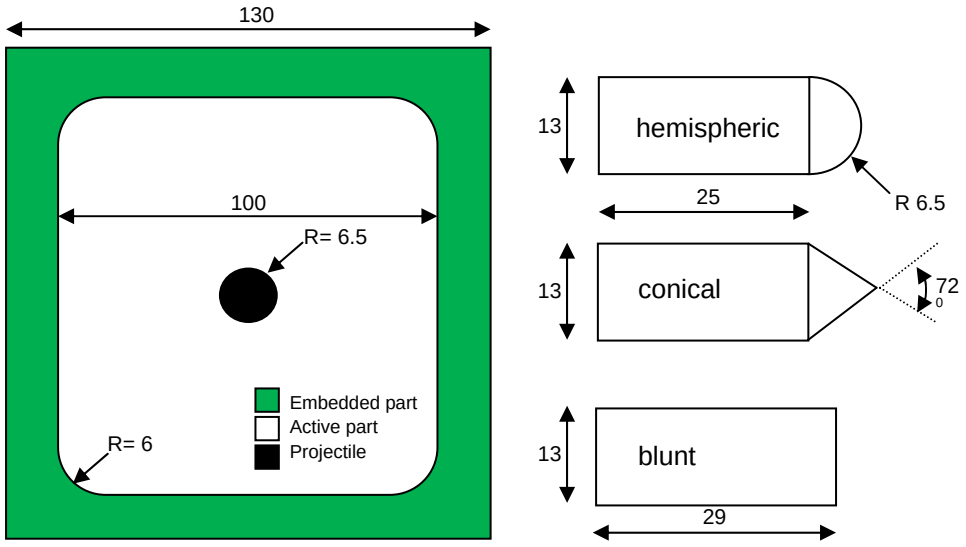

Fig. 1 Geometry of the impacted and perforated steel sheet and of the projectiles

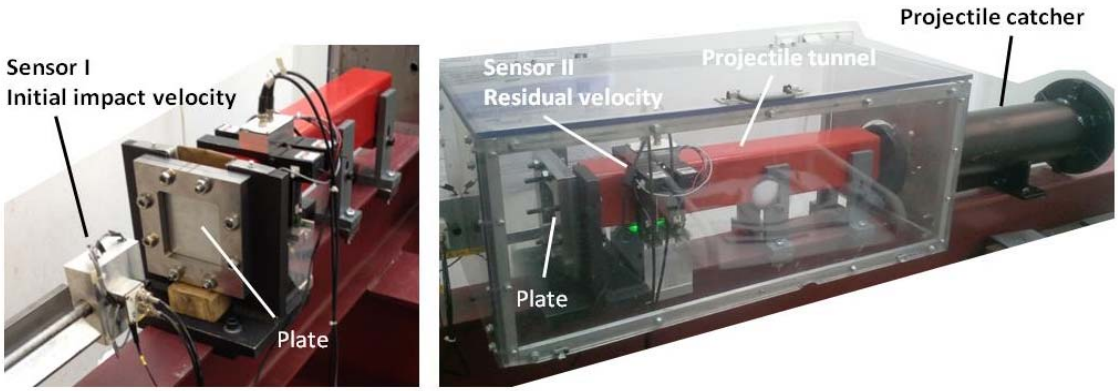

Fig. 2 Experimental setup for ballistic applications

The device, or more precisely the gas gun, used to perform the tests (Kpenyigba 2013) is instrumented with two laser sensors allowing to measure the initial and residual velocities, V_0 and V_R respectively, see Fig. 2. The experiments are performed using three projectile shapes: conical, hemispherical and blunt, see Fig. 1. The mass of the projectile is assumed constant and equal to 30g. The two velocities measured during

the experiments are used to define the ballistic curve $V_R - V_0$. The minimum initial velocity for which the projectile perforates the sheet steel is called ballistic limit V_B. The residual velocities can also be measured using HSC so that a comparison is possible with lasers. In addition, the camera allows to define the failure time t_f for all projectile shapes.

2.2 Results of experiments

Two series of experiments are performed for all three projectile shapes. First, the ballistic curves are obtained using laser sensors. The second series of experiments are performed using HSC to record the perforation process allowing to calculate the failure time for velocities higher than the ballistic limit. Finally, it is possible to calculate the deceleration time of the projectile during perforation using HSC (equal to failure time).

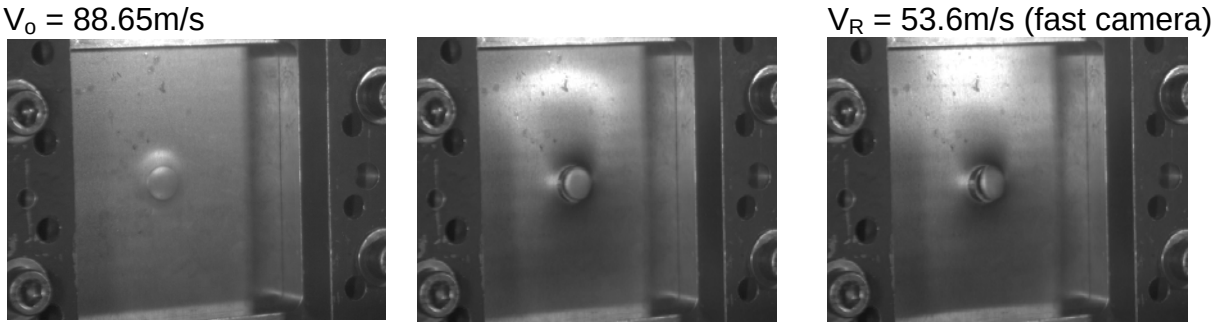

Fig. 3 Perforation process - mild steel sheet perforated by blunt projectile

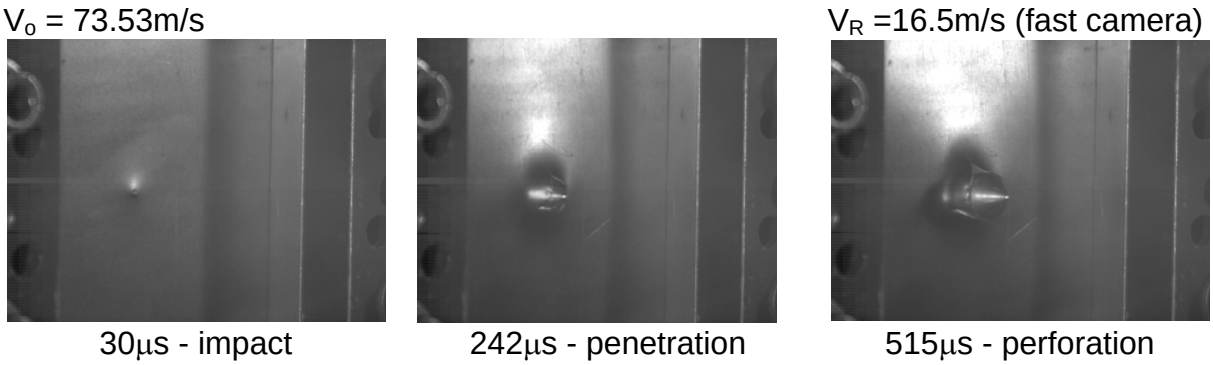

Fig. 4 Perforation process - mild steel sheet perforated by conical projectile

From recorded experiments, only some frames are reported in the paper, Fig. 3, 4 and 5, to explain the basic effects. Fig. 3 refers to blunt projectile and presents three frames corresponding to the perforation process. The velocity measured by the initial velocity sensor is 88.65m/s and the residual velocity measured using the high speed

camera is equal to 53.6m/s. On the left, the frame just after impact (30μs) is visible; on the right, the frame with complete perforation (the projectile nose reaches the opposite side of the sheet) is presented (182μs). In addition, the intermediate frame (151μs) is reported to present the failure evolution during penetration. During perforation, the projectile decelerates from initial to residual velocity in a very short time (182μs). It is possible to predict the impact force level which is transferred from the projectile to the plate as it will be discussed later.

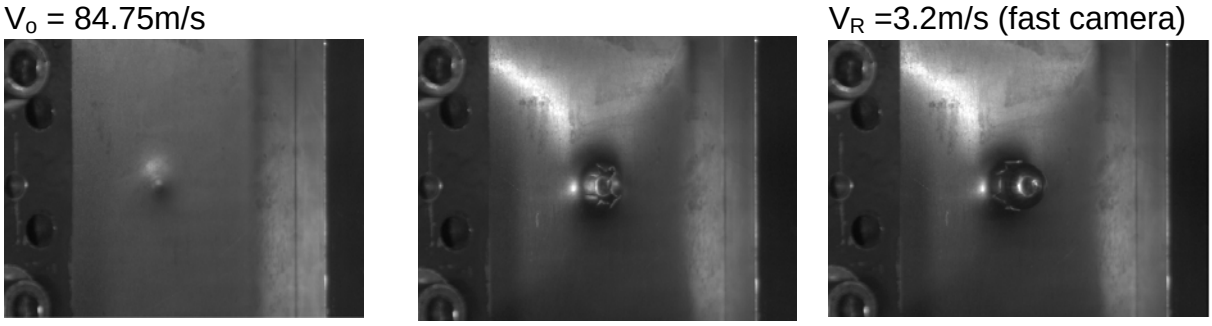

Fig. 5 Perforation process - mild steel sheet perforated by hemispherical projectile

Next figure, Fig. 4, reports the three corresponding frames for conical projectile and an initial velocity equal to 73.53m/s. The residual velocity described by HSC is 16.5m/s. Fig. 5 presents the corresponding experimental results for hemispherical projectile. In this case, the residual velocity is 3.2m/s for an initial velocity equal to 84.75m/s. The low residual velocity means that the result is close to the ballistic limit.

On the following pictures, Fig. 6, the ballistic curves for all the considered projectile shapes are summarized. The ballistic limits are also reported. The data from velocity sensors together with HSC (one point for every projectile shape) are compared. Using experimental results, the relation proposed by Recht and Ipson (Recht 1963) is used to fit the experiments. It is observed a good agreement in all cases.

Different mechanisms of failure are observed during experiments (Kpenyigba 2013) using conical, hemispherical and blunt projectiles, Figs 3, 4 and 5. The conical projectile has an angle of 72°, Fig. 1. However other angles have also been considered. The experiments have shown that increasing the projectile angle induces a decrease of the number of petals. The limit case inducing one plug ejection is estimated at 120°. The detailed presentation of this effect is described in (Kpenyigba 2013). The simulations predict the same number of petals as experiments and in the case of an angle of 72°, the number of petals is 4.

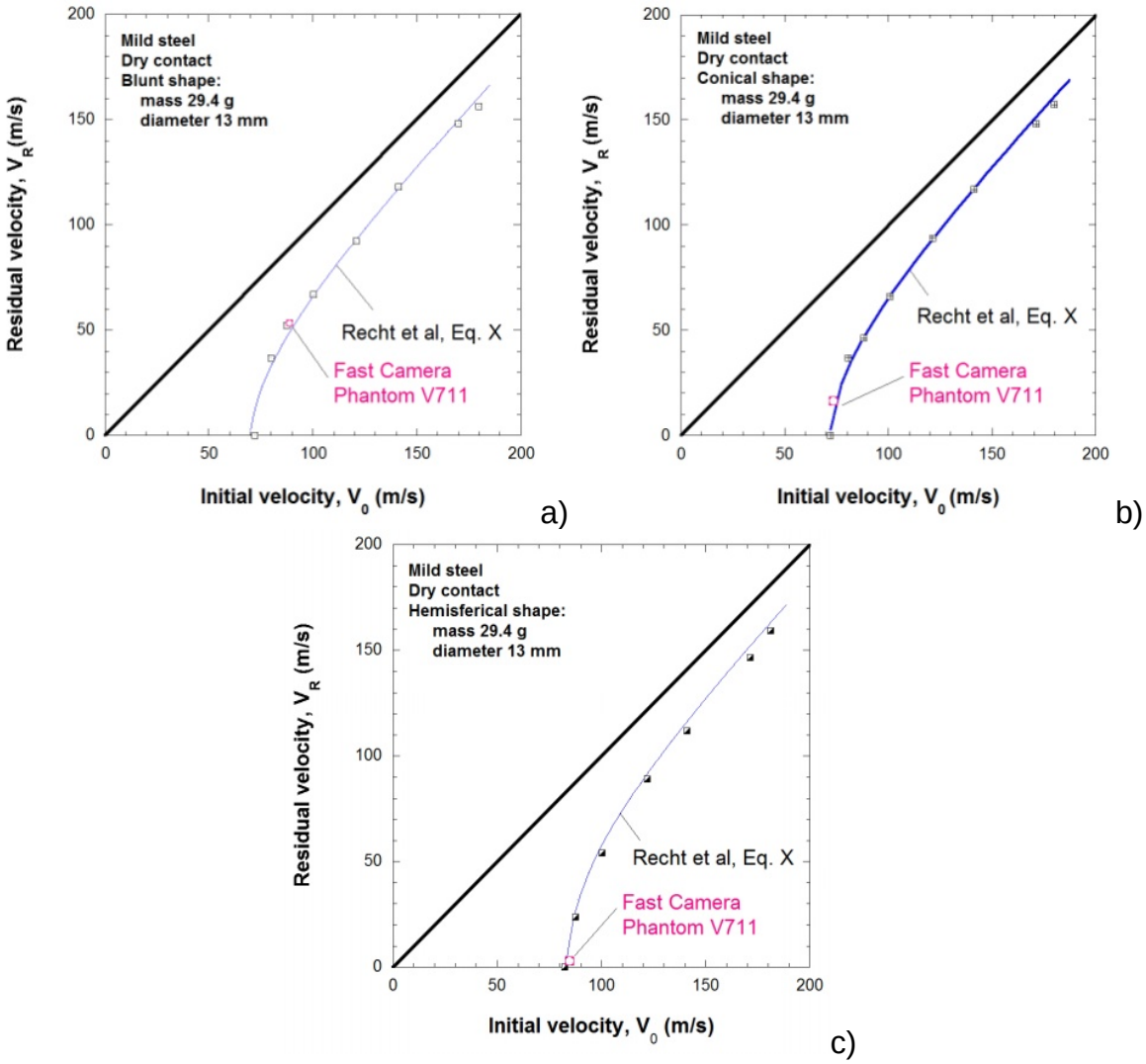

Fig. 6 Ballistic curves-experimental data
a) blunt projectile; b) conical projectile; c) hemispherical projectile

3. NUMERICAL PART

The numerical simulations with Abaqus/Explicit finite element code (Simulia 2011) are used to predict all measurements done during experiments: failure mode, ballistic curve, ballistic limit. In addition, the analysis of impact force is done. The details of the numerical analysis are presented below.

3.1 Numerical model description

The numerical simulations are used to describe the aspects of the experiments which cannot be measured directly in the laboratory, for example the impact force (not possible because we don't have any sensors at the moment but it is possible in a general case), stress, strain, displacement and velocities distribution during the process.

The numerical model used in simulations is presented together with boundary and initial conditions. In addition, the constitutive material model is given together with the material parameters.

The explicit finite method is used to integrate in time domain the equations of motion. Finally, the process of impact, penetration and perforation is simulated and the finite element mesh is shown in Fig. 7. The central part of the model is built with about 110 000 finite elements (five elements along thickness - type: C3D8R - size: 0.2mm) and the exterior part has about 73 000 elements (two elements along thickness - type: C3D8I - size: 0.5mm). It means that the length of finite element in the central zone is 0.2mm but in exterior zone is 0.5mm. In central part, C3D8R are used (five elements along thickness) and in exterior part C3D8I (two elements along thickness). C3D8I are used to model in a better way the bending behavior of the plate. The tie constraint guarantees continuous displacement and stress fields on the border. The fine mesh interior zone of the model have a 30 mm diameter. It allows to initiate the crack propagation in a precise way. The influence of the mesh size was also analyzed.

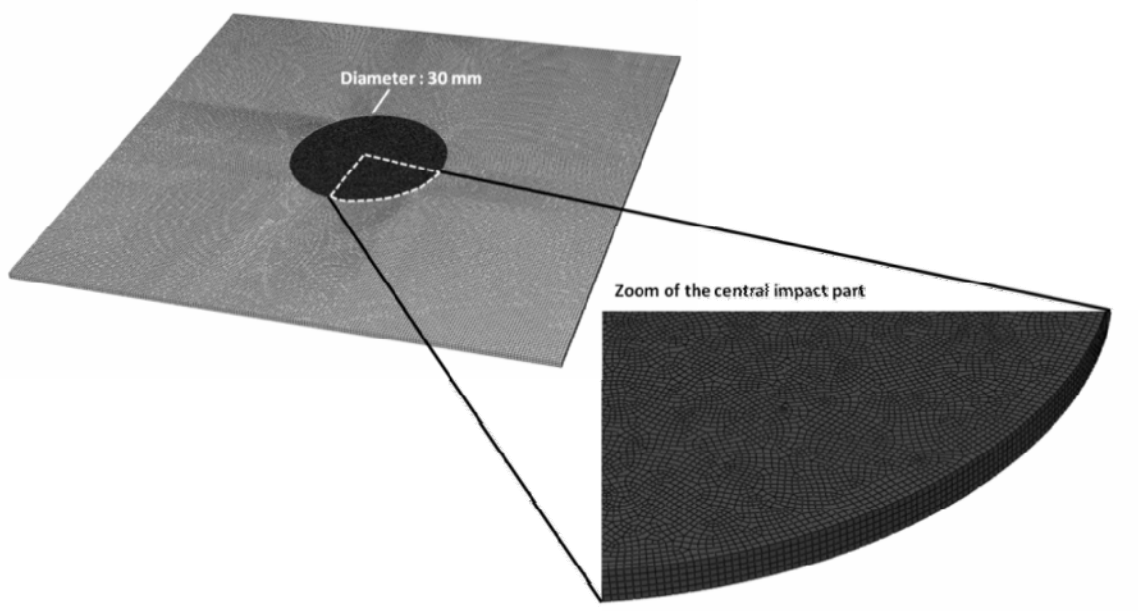

Fig. 7 Finite element mesh used to simulate the process

The mild steel material behavior of the sheet is modeled using a thermoviscoplastic model including strain hardening, strain rate sensitivity and thermal softening. In numerical simulation, the isotropic hardening-softening law proposed by Johnson-Cook (Johnson 1983) was used in the following form, Eq. (1):

$$\sigma = \left(A + B\varepsilon_p{}^n\right)\left[1 + C\ln\left(\frac{\dot{\varepsilon}_p}{\dot{\varepsilon}_0}\right)\right]\left[1 - \left(\frac{T - T_{trans}}{T_{melt} - T_{trans}}\right)^m\right], \quad (1)$$

where σ is the equivalent Mises stress, ε_p is the equivalent plastic strain, $\dot{\varepsilon}_p$ is the equivalent plastic strain rate and T is the actual temperature. The model has five material parameters A, B, n, C and m that describe the yield stress (A), the strain hardening (B and n), the strain rate sensitivity (C) and the thermal softening (m). In addition, the following physical properties should be identified T_{melt} (melting temperature), T_{trans} (transition temperature) and reference strain rate $\dot{\varepsilon}_0$. The increment of the temperature assuming adiabatic conditions is calculated based on following equation, Eq. (2):

$$\Delta T = \frac{\beta}{\rho C_p} \int \sigma d\varepsilon_p, \tag{2}$$

where β is the Quinney-Taylor coefficient, ρ is the density of the material, C_p is the specific heat.

The constants used to describe the thermoviscoplastic behavior are summarized in Tabs 1 and 2. It allows to take into account strain, strain rate and temperature sensitivity.

Tab. 1 All constants for the Johnson-Cook model, Eqs (1) and (2)

A (MPa)	B (MPa)	n (-)	C (-)	$\dot{\varepsilon}_0$ (s^{-1})	T_{trans} (K)	T_{melt} (K)	m (-)
153.82	463.82	0.37	0.02	0.0001	300	1600	0.7

β (-)	C_p ($Jkg^{-1}K^{-1}$)	ρ (kgm^{-3})
0.9	470	7800

Tab. 2 Failure strain and triaxiality dependent on projectile shape

Projectile shape	Blunt	Conical	Hemispherical
Failure strain, ε_f	0.6	1.2	0.65
Triaxiality, $\overline{\eta}$	0	1/3	2/3

It must be noticed that the residual velocity is dependent on the failure strain level ε_f. It is an important parameter and sensitivity analysis is done for all three shapes of projectile, Fig. 9. The optimal values of the failure strains are presented in Tab. 2 for each projectile's shape. During numerical simulations of the process of perforation the triaxiality $\overline{\eta}$ has been estimated, see Tab. 2. It is observed that for blunt projectile

failure mode is due to pure shear ($\overline{\eta} = 0$); for conical, it is related to uniaxial tension ($\overline{\eta} = 1/3$) and for hemispherical to biaxial tension ($\overline{\eta} = 2/3$). All these observations are in agreement with (Lee 2005, Bao 2005).

3.2 Numerical results

It is possible to reproduce numerically all the failure modes observed during experiments, Figs 3, 4 and 5. The comparisons between numerical and experimental results are in agreement, Fig. 8. Concerning the number of petals with the projectile nose angle between 30^0 and 120^0, a good agreement is observed between experiments and numerical simulations.

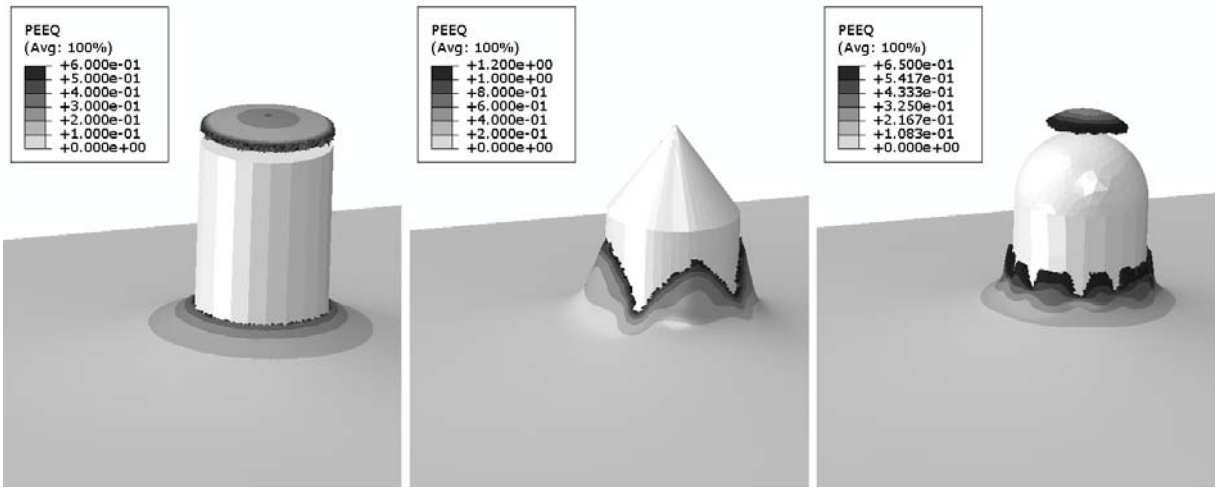

Fig. 8 Failure pattern for conical, hemispherical and blunt projectile shapes, $V_0 = 120\, m/s$.

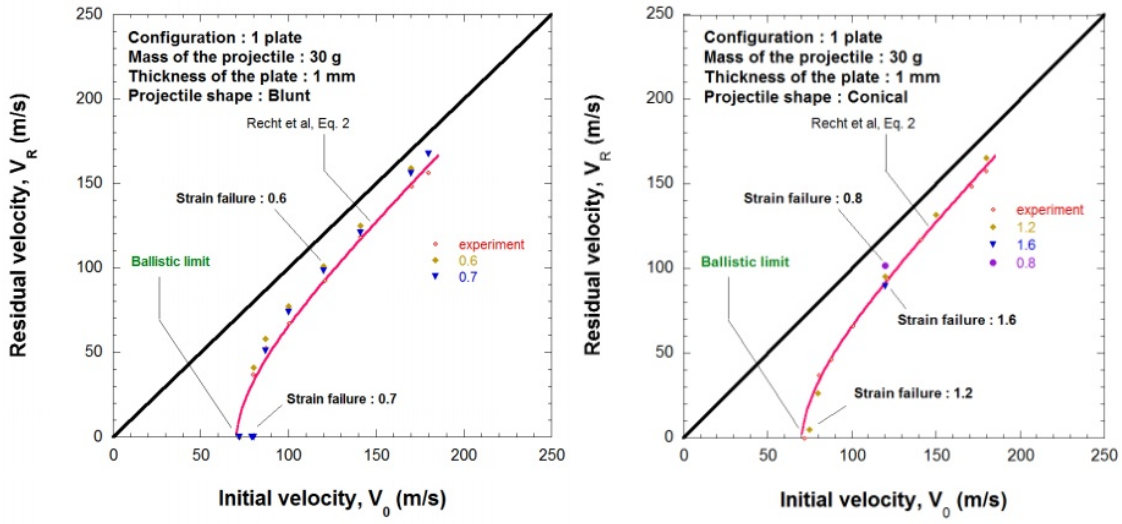

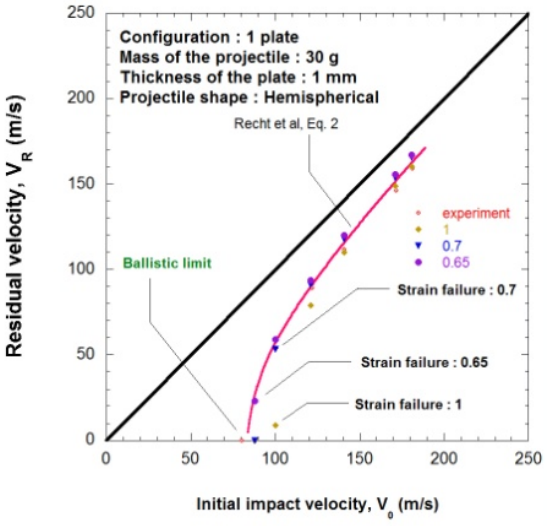

Fig. 9 The comparison of ballistic curves from experiments and from simulation for all projectile shapes

Finally, the ballistic curves are presented for all considered projectile shapes. The numerically obtained results are in good agreement with experimental data, Fig. 9.

3.3 Failure time

The important aspect analyzed very often during the perforation process is the failure time, it means the time for complete perforation of the plate as it is defined on the right side of Figs 3, 4 and 5. The time resolution of high speed camera is about 30μs but the resolution of the numerical model is depends on the initial velocity. During our perforation tests, it corresponds to 20 frames but of course the process is shorter for higher initial velocities and longer for lower impact velocities. Finally, the time resolution of numerical simulations is between 10μs and 50μs.

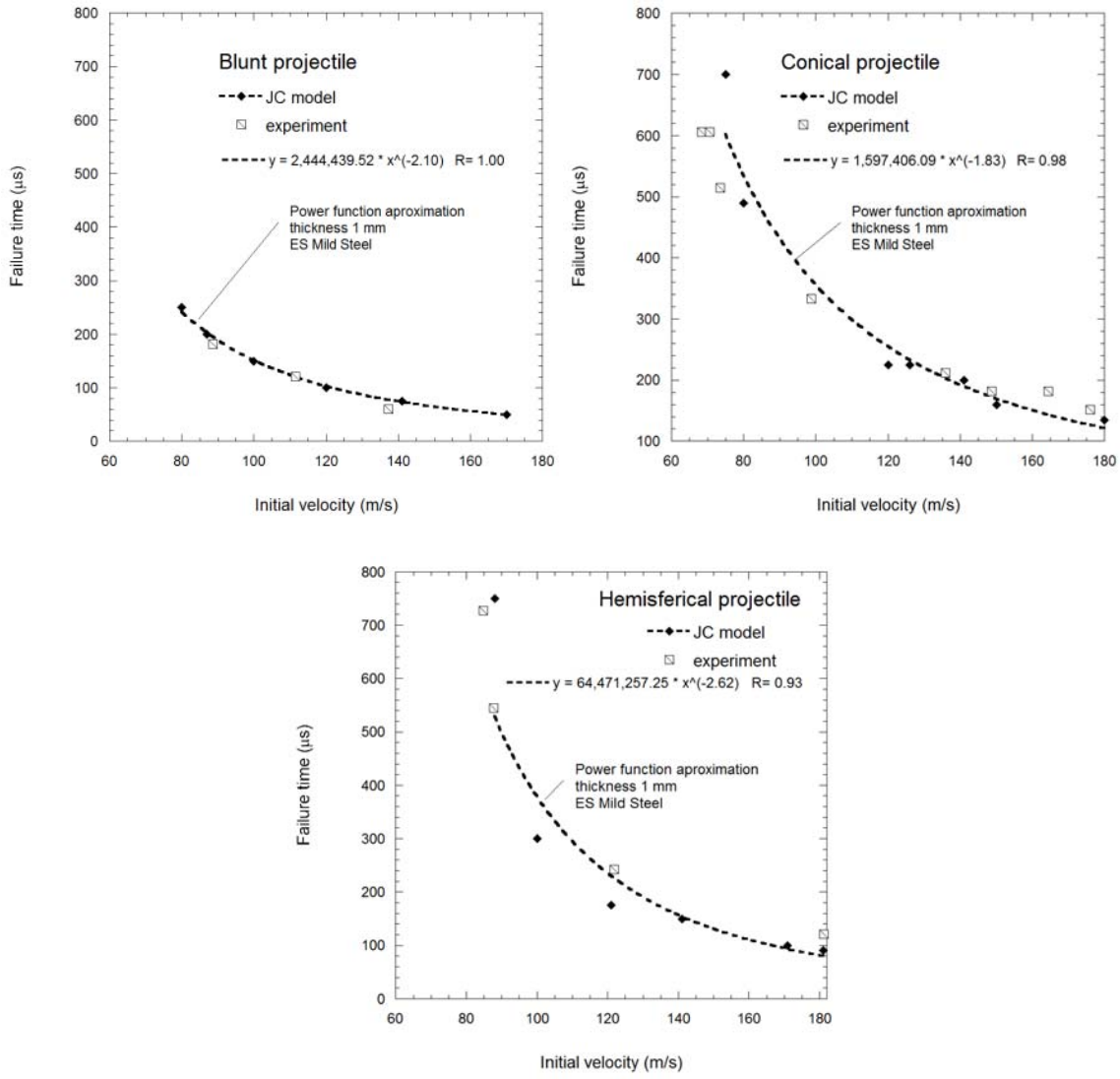

Fig. 10 Comparison of failure time in experiments and in numerical simulations for different projectile shapes

The curves describing these relationships for all three considered projectile shapes are presented in Fig. 10. The agreement is acceptable taking into account possible errors from time resolution of the high speed camera and numerical model. The important idea is that the same methodology is used in both types of analyses.

3.4 Impact force

The force of the impact is also analyzed in the paper. During previous experiments, it was not possible to measure the force because of a lack of appropriate equipment. However it is possible to predict numerically the impact force which is generally nonlinear impulse during perforation, see Fig. 11. In simulations the description of the impact force history does not pose any problem. As was discussed above, it is possible

to describe in simulations some points on ballistic curve for which coordinates are initial velocity and residual velocity, see Fig. 9. The perforation time can be also described; it is connected with deceleration of the rigid projectile, Fig. 10. Of course the observed perforation time in virtual experiments is longer than the real deceleration time which is equal to the time when the force is greater than zero, see Fig. 10. The problem is time resolutions for experiments (HSC) and numerical simulations (20 frames during the process), see point 3.3.

Type	Initial Velocity (m/s)	Residual Velocity (m/s)	MF (N)	MTP (μs)	OTP (μs)	AF (N)	TF (N)
Sim	88.000	23.040	9310	490	750	3820	2598
Exp	87.720	23.830	-	-	545	-	3516
Sim	121.00	93.770	9620	190	175	4070	4668
Exp	121.95	89.16			242		4065

Notation:
MF – Maximum Force
MTP – Measured Time of Perforation
OTP – Observed Time of Perforation
AF – Average Force (from MF)
TF – Theoretical Force

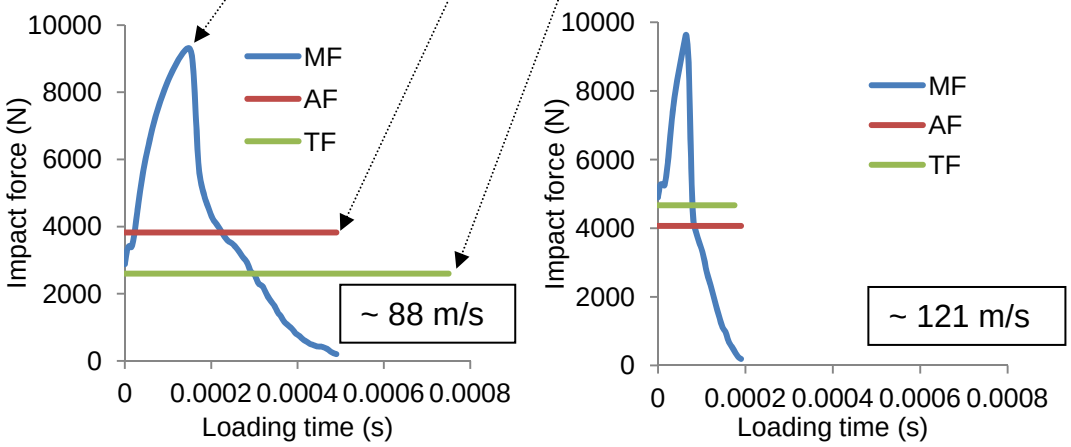

Fig. 11 Impact force for hemispherical projectile - numerical prediction

The theoretical force TF which is imposed to the structure during impact loading can be calculated based on the following formulation, Eq. (3):

$$TF = \frac{V_R - V_0}{t_F} m_p, \tag{3}$$

where TF can be calculated based on numerical simulations or using experiments, knowing the failure time t_F, the initial velocity V_0, the residual velocity V_R and the mass of the projectile m_p. In the previous case, Fig. 11, all necessary data are reported and the mass of the projectile is assumed equal to 30g. For this case (hemispherical projectile and low impact velocity), the theoretical force and the failure time are in acceptable agreement, Fig. 11. For initial velocity close to 88 m/s, the theoretical force (TF) was 2598N in simulation and 3516N in experiment. For the higher velocity close to 121m/s, the theoretical force was 4668N and 4065N using the same methodology. However both are far from the real maximal value of forces in both cases 9310N and 9620N. It seems that only using the force sensors (future work) will give correct description. It can be later compared with the time history of the impact force obtained in simulation MF.

4. CONCLUSIONS

In this paper, a complete analysis of the perforation process is reported. Coupling an experimental approach to numerical simulations, fundamental quantities can be measured and analyzed. It allows a better understanding the perforation mechanisms. Moreover, a good agreement is observed between experiments and numerical results.

Through experiments, it is observed that the projectile shape is changing the failure mode and the failure strain level. It is due to the stress triaxiality state as reported in (Kpenyigba 2013). The failure time was studied and in all cases, a parabolic decrease is observed with the impact velocity. It was also observed during tests that the nose angle using a conical shape is changing the number of petals corresponding to radial cracks.

In addition, based on failure time as well as initial and residual velocities, the impact force was predicted (numerically and experimentally). The real time history of the impact force was also defined in simulations and the conclusion is that it is far from the theoretical value. The reason is that the deceleration of the projectile is not constant during perforation.

REFERENCES

Simulia (2012), *Abaqus Analysis User's Manual*, HTML version 6.12.

Alavi Nia A., Hoseini G.R. (2011), "Experimental study of perforation of multi-layered targets by hemispherical-nosed projectiles", *Materials and Design*, **32**(2), 1057–1065.

Atkins A. G., Afzal Khan M., M. Liu J. H. (1998), "Necking and radial cracking around perforations in thin sheets", *International Journal of Impact Engineering* , **21**(7), 521-539.

Borvik T., Langseth M., Hoperstad O.S., Malo K.A. (2002), "Perforation of 12 mm thick steel plates by 20 mm diameter projectiles with flat, hemispherical and conical noses part I: experimental study", *International Journal of Impact Engineering*, **27**, 19–35.

Dean J., Dunleavy C.S., Brown P.M., Clyne T.W. (2009), “Energy absorption during projectile perforation of thin steel plates and the kinetic energy of ejected fragments”, *International Journal of Impact Engineering*, **36**, 1250–1258.

Dey S., Borvik T., Hopperstad O.S., Leinum J.R., Langseth M. (2004), “The effect of target on the penetration of steel plates using three different projectile nose shapes”, *International Journal of Impact Engineering*, **30**, 1005–38.

Jankowiak T., Rusinek A., Lodygowski T., 2011, Validation of the Klepaczko–Malinowski model for friction correction and recommendations on Split Hopkinson Pressure Bar, *Finite Elements in Analysis and Design*, **47**, 1191–1208.

Jankowiak, T., Rusinek, A., Wood, P. (2013), “A numerical analysis of the dynamic behaviour of sheet steel perforated by a conical projectile under ballistic conditions”, *Finite Elements in Analysis and Design*, **65**, 39–49.

Johnson G.R., Cook W.H. (1983), “A constitutive model and data for metals subjected to large strains, high strain rates and high temperatures”, *Proceedings of 7th international symposium on ballistics*, Hague.

Kpenyigba, M., Jankowiak, T., Rusinek, A., Pesci, R. (2013), “Influence of projectile shape on dynamic behavior of steel sheet subjected to impact and perforation”, *Thin-Walled Structures*, **65**, 93–104.

Lee Y.W., Wierzbicki T. (2005), “Fracture prediction of thin plates under localized impulsive loading. Part II: discing and pedalling”, *International Journal of Impact Engineering*, **31**, 1277–308.

Recht, R.F., Ipson, T.W. (1963), “Ballistic perforation dynamics”, *J. Appl. Mech*., **30**, 384.

Rusinek A. (2000), “Modélisation thermoviscoplastique d’une nuance de tôle d’acier aux grandes vitesses de déformation. Etude expérimentale et numérique du cisaillement, de la traction et de la perforation”, *Ph.D. thesis*, Université du Metz.

Rusinek A., Zaera R., Klepaczko J.R. (2007), “Constitutive relations in 3-D for a wide range of strain rates and temperatures – Application to mild steels”, *International Journal of Solids and Structures*, **44**(17), 5611-5634.

Scheffler D.R., Zukas J.A. (2000), “Practical aspects of numerical simulations of dynamic events: effects of meshing”, *International Journal of Impact Engineering*, **24**(9), 925–45.

Zukas J.A., Scheffer D.R. (2001), “Impact effects in multilayered plates”, *International Journal of Solids and Structures*, **38**(19), 3321-3328.